COMMUNICATION

ChemComm
www.rsc.org/chemcomm

Super-hydrophobic tin oxide nanoflowers

Aicheng Chen,* Xinsheng Peng, Kallum Koczkur and Brad Miller
Department of Chemistry, Lakehead University, Thunder Bay, Ontario, Canada P7B 5E1.
E-mail: aicheng.chen@lakeheadu.ca

Received (in Cambridge, UK) 18th May 2004, Accepted 8th June 2004
First published as an Advance Article on the web 15th July 2004

Super-hydrophobic 3D SnO_2 flowers with nanoporous petals were produced from the 3D Sn nanoflowers using a controlled shape-preserving thermal oxidation process.

Size, shape and dimensionality strongly affect the properties of nanomaterials. A three-dimensional (3D) integrated platform of nanostructured metallic or semiconducting materials is highly desirable for advanced nanoscale electronic and optoelectronic applications.[1] Being a smart semiconductor, tin dioxide (SnO_2) has attracted much attention due to its broad application in many fields, for instance surface coatings, selective gas sensors and lithium secondary batteries.[2–4] Apart from nanoparticles, different one-dimensional (1D) SnO_2 nanostructures such as nanoribbons, nanotubes, nanorods and nanowires have been fabricated by physical/chemical vapor deposition processes,[5,6] the solution-based method[7a] and an anodic oxidation technique.[7b] However, there is no report on 3D porous SnO_2 nanostructures. In this communication, we report for the first time the synthesis of 3D SnO_2 nanoflowers with nanoporous petals produced from the 3D Sn nanoflowers using a controlled structure-preserving thermal oxidation process.

The 3D Sn nanoflowers were formed on a titanium substrate by thermal-pyrolysis of a tin organometallic precursor dibutyltin dilaurate (DBTDL). Briefly, titanium plates ($30 \times 15 \times 0.8$ mm^3) were pretreated as follows: degreased using acetone, etched in a 30 wt% HCl solution at 80 °C for 10 min to remove the titanium oxide layer, then dried in a vacuum oven at 40 °C. A thermal pyrolysis procedure was performed in a horizontal tube furnace equipped with a ceramic tube. The pretreated Ti substrate and a ceramic boat containing the tin organometallic precursor were put into the ceramic tube. Before heating, a constant stream of ultrapure argon (99.999%) at a flow rate of 200 sccm was introduced into the system for 4 h. Then the furnace was heated up to 350 °C at a rate of 50 °C min^{-1}. The temperature was kept at 350 °C for 1.5 h, and then naturally cooled to room temperature. During the heating and cooling processes, the flow rate of the ultrapure argon was maintained at 100 sccm. The thermal oxidation process approximating rheotaxial growth and thermal oxidation (RGTO)[8,9] was used to convert the metallic 3D Sn nanoflowers to 3D SnO_2 nanoflowers. Before carrying out complete oxidation of the Sn nanoflowers at 500 °C for 6 h in air, a thin supporting tin oxide skin was grown on the surface of the tin nanoflowers in air for 2 h at 200 °C. This deliberate and crucial step was taken to maintain the shape and integrity of the as-synthesized tin nanostructures during the conversion of Sn into SnO_2 as the melting point of tin is low (232 °C).

Fig. 1 shows scanning electron microscopy (SEM) images of the as-synthesized Sn nanostructures. A large number of Sn nanoflowers were formed as shown in Fig. 1a. More detailed morphologies of the flower-like nanostructures with porous nanopetals are shown in Fig. 1b and 1c. Fig. 1b shows that several dozens of porous nanopetals connect with each other forming 3D nanoflowers by self-assembly. These Sn nanopetals are about 50 nm thick, tens of μm wide and Fig. 1c reveals that they are porous with random holes having diameters between tens and several hundreds of nanometers. After the RGTO oxidation, the as-synthesized 3D Sn nanoflowers were completely converted into SnO_2 3D nanoflowers without any obvious shape change. The 3D SnO_2 nanoflowers observed in Fig. 1d and 1e are very similar to the 3D Sn nanostructures seen in Fig. 1a and 1b. However, the high-magnification SEM images (Fig. 1c and 1f) reveal that the SnO_2 nanopetal porosity is greatly increased when compared with the as-synthesized nanopetals of the Sn nanoflowers.

X-ray diffraction (XRD) analysis was used to further investigate the change of the composition and structure of the 3D nanoflowers upon RGTO oxidation. Typical XRD patterns of the Sn nanoflowers and the 3D SnO_2 nanostructures are shown in Fig. 2. All the peaks marked by a star are derived from the titanium substrate. Fig. 2a reveals that the as-prepared Sn nanoflowers are in the β-tin

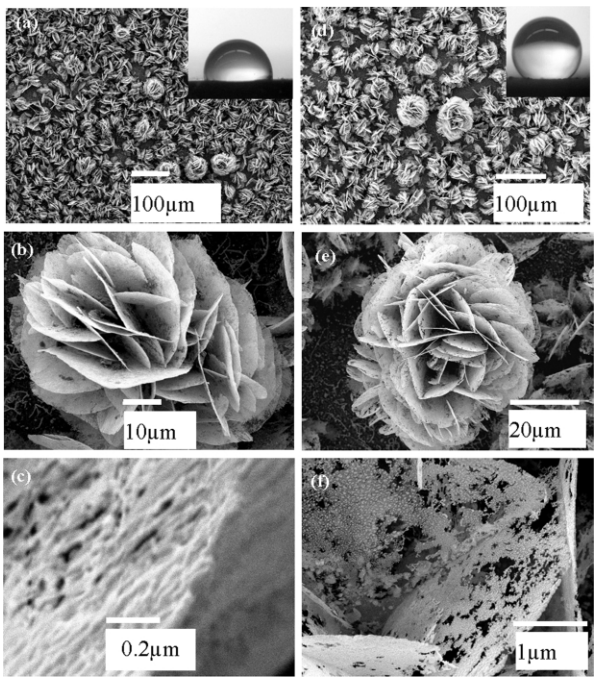

Fig. 1 SEM images (a) low magnification, (b) individual flower-like structure, (c) one piece of a porous nanopetal of the as-prepared Sn nanoflowers; (d) low magnification, (e) typical flower-like morphology, (f) high-magnification of the petals of SnO_2 formed by the RGTO process. The insets are the shapes of water droplets on the corresponding surfaces.

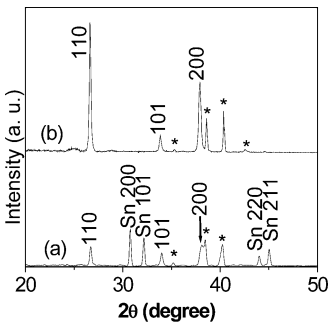

Fig. 2 XRD patterns of (a) the as-synthesized tin nanostructures, (b) after complete RGTO oxidation.

DOI: 10.1039/b407313d

phase. The weak peaks (110), (200) and (101) of SnO_2 indicate that the Sn flowers are partially oxidized in air. This is consistent with the observation that tin oxide is formed on the surface of Sn nanowires due to oxidation in air at room temperature.[9] As seen in Fig. 2b, all peaks arising from tin disappear after RGTO oxidation, which indicates that the tin is completely oxidized into SnO_2. The XRD patterns further show that the formed SnO_2 has the cassiterite structure. Please note that tin suboxide is not observed in the formed tin oxide nanoflowers due to the 6 h long oxidation at 500 °C in air.

Fig. 3 shows transmission electron microscopy (TEM) images and corresponding high resolution TEM images of the nanopetals of the nanoflowers. The as-prepared nanopetals of the Sn flowers (Fig. 3a) and the post-annealed nanopetals of the SnO_2 nanoflowers (Fig. 3d) are porous. The shapes and the sizes of the pores are irregular. Comparison of Fig. 3a and 3d reveals that the average pore size of the Sn nanopetals is smaller than that of the SnO_2 nanopetals, in good agreement with the SEM observations. In addition, Fig. 3a shows core–shell structures caused by a thin oxide layer covering the tin nanopetal. Their structure and composition are further characterized using HRTEM and energy dispersive X-ray spectroscopy analysis (EDS). Fig. 3b indicates that the interlayer spacing is about 0.28 nm, close to the *d* value (0.2793 nm) of the (101) plane of β-tin. Fig. 3c shows that these nanopetals are composed of 97.76 at% Sn and 2.24 at% oxygen. Fig. 3e and 3f indicate that SnO_2 is formed with an interlayer space of 0.35 nm, attributed to the (110) plane of cassiterite SnO_2 and that the element composition is 33.48 at% Sn and 66.52 at% O, close to the ratio of 1 : 2 in the bulk SnO_2 showing that Sn is completely oxidized into SnO_2.

The above results suggest that the growth of Sn flower nanopetals is probably controlled by a vapor–solid (VS) process.[6] The tin vapor is formed from the pyrolysis of DBTDL first and then carried by the Ar stream to the low temperature zone, where it deposits on the Ti substrate, nucleates and self-assembles into networks forming the 3D nanoflowers. In the initial stages, the interplay between the dynamic wetting behavior and thermally-enhanced surface diffusion of tin adatoms on the substrate may facilitate the formation of the network patterns, rather than forming isolated droplets or a continuous film, at the elevated temperature. Although further investigation is necessary to elucidate the mechanism of the growth of the 3D tin nanoflowers, we believe that the formation of the tin nanoflowers is initiated along the grain boundaries as these are the most thermodynamically active sites for the precipitation of tin atoms, similar to the grain boundary formation of ZnO nanowalls.[1]

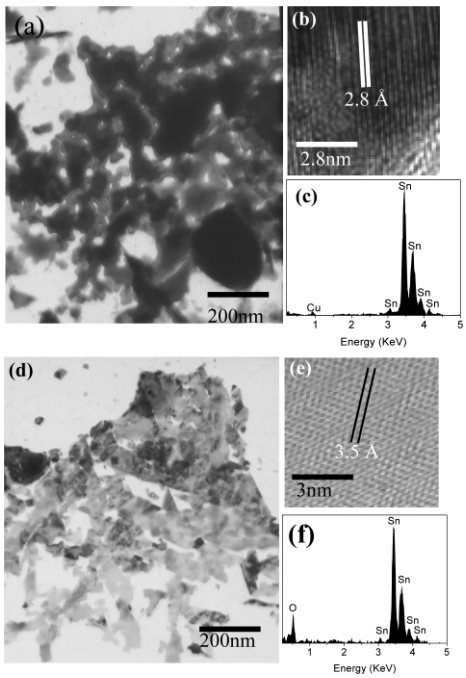

Fig. 3 (a) Low magnification TEM image, (b) and (c) are the corresponding HRTEM and EDS of the as-prepared tin nanostructures, respectively. The peak of copper was derived from Cu grids. (d) A typical TEM image, (e) and (f) are the corresponding HRTEM and EDS of the completely oxidized products.

We further investigated the wetting properties of the Sn and SnO_2 nanoflowers. The water contact angle is 90° for the Sn nanoflowers (Fig. 1a) and 155° for the SnO_2 flowers (Fig. 1b). In contrast, we found the water contact angle is around 60° for a smooth Sn surface and about 90° for a flat SnO_2 surface. These results show that the water contact angle of the nanoflower surfaces is much larger than that of the corresponding smooth surfaces, suggesting that the significant increase of hydrophobicity results from the dramatic change of the surface structure and roughness. This observation is consistent with Cassie and Baxter's model,[10] which describes the contact angle at a heterogeneous surface composed of different materials, in our case, the trapped air in the hollows and Sn or SnO_2 nanoflowers. The super-hydrophobicity of SnO_2 nanoflowers originates from the contribution of the air trapped in the interspaces of rough surfaces similar to that of well-aligned nanorod TiO_2 arrays.[11]

In summary, 3D Sn nanoflowers and 3D SnO_2 nanoflowers were successfully synthesized in this study; Ti is favorable for the formation of Sn nanoflowers compared with other substrates such as ceramic Al_2O_3 and Sn. The dimensions of the nanopetals depend on the applied temperature and the flow rate of argon. The preservation of the shape of individual nanopetals as well as the morphology of an entire 3D nanoflower upon oxidation suggests a promising route for fabricating other 3D oxide nanonatures from their 3D metal nanomaterials. The super-hydrophobic 3D SnO_2 nanoflowers with porous nanopetals possess a very high surface-to-volume ratio, which is especially desirable for sensor design in moisture environments.

This work was supported by the Natural Sciences and Engineering Research Council of Canada (NSERC). A. Chen acknowledges the Ontario Premier's Research Excellence Award.

Notes and references

1 H. T. Ng, J. Li, M. K. Smith, P. Nguyen, A. Cassell, J. Han and M. Meyyappan, *Science*, 2003, **300**, 1249.
2 T. Sahm, L. Mädler, A. Gurlo, N. Barsan, S. E. Pratsinis and U. Weimar, *Sens. Actuators, B*, 2004, **98**, 148.
3 E. Comini, V. Guidi, C. Malagù, G. Martinelli, Z. Pan, G. Sberveglieri and Z. L. Wang, *J. Phys. Chem. B*, 2004, **108**, 1882.
4 D. S. Torkhov, A. A. Burukhin, B. R. Churagulov, M. N. Rumyantseva and V. D. Maksimov, *Inorg. Mater.*, 2003, **39**, 1342.
5 M. Law, H. Kind, B. Messer, F. Kim and P. D. Yang, *Angew. Chem., Int. Ed.*, 2002, **41**, 2405.
6 Z. R. Dai, J. L. Gole, J. D. Stout and Z. L. Wang, *J. Phys. Chem. B*, 2002, **106**, 1274.
7 (*a*) F.-F. Zhang, L.-D. Sun, J.-L. Yin and C.-H. Yan, *Adv. Mater.*, 2002, **15**, 1022; (*b*) H-C. Shin, J. Dong and M. L. Liu, *Adv. Mater.*, 2004, **16**, 237.
8 T. Aste, D. Beruto, R. Botter, C. Ciccarelli, M. Giordani and P. Pozzolini, *Sens. Actuators, B*, 1994, **19**, 637.
9 A. Kolmakov, Y. X. Zhang and M. Moskovits, *Nano Lett.*, 2003, **3**, 1125.
10 A. B. D. Cassie and S. Baxter, *Trans. Faraday Soc.*, 1944, **40**, 54.
11 X. Peng and A. Chen, *J. Mater. Chem.*, 2004, DOI: 10.1039/b404750h.